ELEMENTA
Science of the Anthropocene

Oak, YJ, et al. 2019. Evaluation of simulated O_3 production efficiency during the KORUS-AQ campaign: Implications for anthropogenic NO_x emissions in Korea. *Elem Sci Anth,* 7: 56. DOI: https://doi.org/10.1525/elementa.394

RESEARCH ARTICLE

Evaluation of simulated O_3 production efficiency during the KORUS-AQ campaign: Implications for anthropogenic NO_x emissions in Korea

Yujin J. Oak*, Rokjin J. Park*, Jason R. Schroeder†,‡, James H. Crawford†, Donald R. Blake§, Andrew J. Weinheimer‖, Jung-Hun Woo¶, Sang-Woo Kim*, Huidong Yeo*, Alan Fried**, Armin Wisthaler††,‡‡ and William H. Brune§§

We examine O_3 production and its sensitivity to precursor gases and boundary layer mixing in Korea by using a 3-D global chemistry transport model and extensive observations during the KORea-US cooperative Air Quality field study in Korea, which occurred in May–June 2016. During the campaign, observed aromatic species onboard the NASA DC-8 aircraft, especially toluene, showed high mixing ratios of up to 10 ppbv, emphasizing the importance of aromatic chemistry in O_3 production. To examine the role of VOCs and NO_x in O_3 chemistry, we first implement a detailed aromatic chemistry scheme in the model, which reduces the normalized mean bias of simulated O_3 mixing ratios from –26% to –13%. Aromatic chemistry also increases the average net O_3 production in Korea by 37%. Corrections of daytime PBL heights, which are overestimated in the model compared to lidar observations, increase the net O_3 production rate by ~10%. In addition, increasing NO_x emissions by 50% in the model shows best performance in reproducing O_3 production characteristics, which implies that NO_x emissions are underestimated in the current emissions inventory. Sensitivity tests show that a 30% decrease in anthropogenic NO_x emissions in Korea increases the O_3 production efficiency throughout the country, making rural regions ~2 times more efficient in producing O_3 per NO_x consumed. Simulated O_3 levels overall decrease in the peninsula except for urban and other industrial areas, with the largest increase (~6 ppbv) in the Seoul Metropolitan Area (SMA). However, with simultaneous reductions in both NO_x and VOCs emissions by 30%, O_3 decreases in most of the country, including the SMA. This implies the importance of concurrent emission reductions for both NO_x and VOCs in order to effectively reduce O_3 levels in Korea.

Keywords: Ozone; Ozone production efficiency (OPE); KORUS-AQ; Chemical Transport model

1. Introduction

Air pollution in East Asia has been an important issue especially for densely populated mega-cities with the rapid development over the past few decades. Although stringent air pollution controls have been executed in countries including Japan, Korea, and recently China, surface ozone (O_3), which is a key secondary air pollutant that affects human health and the ecosystem, has shown an increasing trend over the past two decades (2000–2017) (Chang et al., 2017; Li et al., 2019). Moreover, key controlling factors for the O_3 formation still remain uncertain especially in East Asia (Park and Kim, 2014).

O_3 is photochemically produced in the lower troposphere from the oxidation of volatile organic compounds (VOCs) in the presence of nitrogen oxides (NO_x = NO + NO_2) (WHO, 2003). Identifying sources of O_3 precursors and quantifying the effect of the reduction of emissions on ambient O_3 levels are necessary to address the environmental threat that O_3 pollution poses to the public.

Reducing precursor emissions does not always lead to a reduction in O_3 levels because of the nonlinear relationship of O_3 with its precursor concentrations (Lin et al., 1988). The Korean government has put an effort on regulating major emission sectors such as mobile and industrial sources since the 1990s. As a result, emissions and ambient concentrations of NO_x and VOCs showed significant

* School of Earth and Environmental Sciences, Seoul National University, Seoul, KR
† NASA Langley Research Center, Hampton, Virginia, US
‡ California Air Resources Board, Sacramento, California, US
§ Department of Chemistry, University of California at Irvine, Irvine, California, US
‖ National Center for Atmospheric Research, Boulder, Colorado, US
¶ Department of Advanced Technology Fusion, Konkuk University, Seoul, KR
** Institute of Arctic and Alpine Research, University of Colorado, Boulder, Colorado, US
†† Department of Chemistry, University of Oslo, Oslo, NO
‡‡ Institute for Ion Physics and Applied Physics, University of Innsbruck, Innsbruck, AT
§§ Department of Meteorology and Atmospheric Science, Pennsylvania State University, University Park, Pennsylvania, US
Corresponding author: Rokjin J. Park (rjpark@snu.ac.kr)

decreases in the Seoul Metropolitan Area (SMA), where almost half the population reside in (Kim and Lee, 2018). However, despite the successful reductions of precursor emissions, urban O_3 levels have consistently increased nationwide during the past two decades (Susaya et al., 2013). Therefore, understanding the regional characteristics of photochemical O_3 production based on the ambient VOCs or NO_x concentrations is essential to formulate an effective control policy (Liu et al., 1987).

There have been several studies using observed O_3, NO_x, and total reactive nitrogen (NO_y) from field campaigns to investigate the features of O_3 production in both rural, urban, and industrial areas in the United States and Europe (Imhoff et al., 1995; Kleinman et al., 1994; Nunnermacker et al., 2000; Olszyna et al., 1994; Rickard et al., 2002; Trainer et al., 1993). In Korea, most studies have focused on identifying the contribution of various chemical and physical factors to explain O_3 production characteristics in the SMA, as the increasing trend in ground level O_3 is more evident in urban areas (Lee et al., 2007; Ryu et al., 2013). Kim et al. (2018) stated that the increasing trend of O_3 is mainly because of NO_x reductions, and Shin et al. (2013) suggested a control strategy on solvent and traffic emissions of VOCs to reduce O_3 levels in Seoul. Susaya et al. (2013) extended the study on ground level O_3 in Seoul and conducted a trend analysis of urban air quality for six additional major cities, but did not cover any suburban or rural areas.

Along with observations, chemical transport models (CTMs) and box model simulations have been used to test the nonlinear sensitivity of O_3 production to ambient conditions (Kleinman et al., 2002; Mazzuca et al., 2016; Ninneman et al., 2017; Zaveri et al., 2003). CTMs have been used as an effective tool for evaluating the emissions inventory and testing the atmospheric response to changes in precursor emissions (Jeong et al., 2012; Kim et al., 2015; Kim, 2011). However, simulated O_3 concentrations in Korea and East Asia have generally been underestimated in CTMs (Han et al., 2008; Kang et al., 2016), which might be due to a combination of several factors including horizontal and vertical resolutions, uncertainty in meteorological parameters, vertical mixing schemes, and chemical mechanisms (Han et al., 2008; Kang et al., 2016).

In this study, we examine the characteristics of photochemical O_3 production in Korea using aircraft (DC-8) measurements during the international KORea-US cooperative Air Quality field study in Korea (KORUS-AQ). During the campaign, high O_3 episodes exceeding 100 ppbv were reported along with high levels of reactive precursor (e.g., NO_x, aromatic VOCs) mixing ratios. We compare the results of an observation-constrained 0-D photochemical box model with a 3-D global CTM to analyze the sensitivity of O_3 production to various atmospheric processes including chemical mechanisms, emissions, and vertical mixing. We also conduct several sensitivity simulations by perturbing emissions of O_3 precursors and suggest the possible implication for future O_3 levels based on the emissions reduction plan by the Korean Ministry of Environment.

2. Methods

2.1 KORUS-AQ field campaign

The atmospheric chemical composition over the Korean peninsula is influenced by a combination of many different sources. Due to the high population density, local anthropogenic emissions are dominant in urban cities, such as the SMA and Busan. Local emissions from power plants, petrochemical and other manufacturing industries also affect regional air quality (NIER and NASA, 2017). Furthermore, a large proportion of the country is covered with mountains, which serve as a profound source of biogenic emissions (Kim et al., 2014) (**Figure 1**). Meanwhile, due to the geographic location and meteorological conditions, Korea is often influenced by anthropogenic emissions and soil dust transported from China (Lee et al., 2019) and biomass burning from Siberia (Jung et al., 2016).

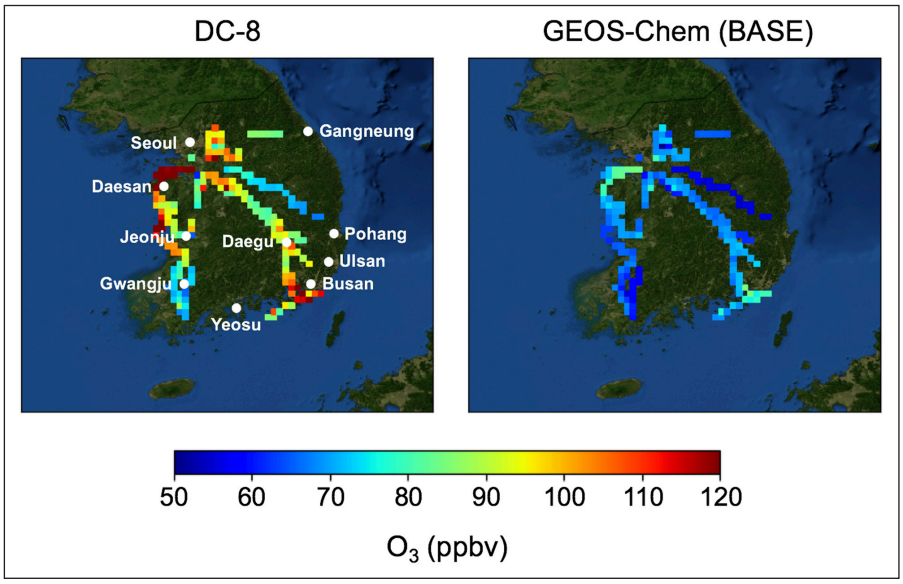

Figure 1: Spatial distribution of observed and simulated O_3. Spatial distribution of the observed and simulated O_3 mixing ratios along the DC-8 flight track during 13–16 LST (averaged below 1.5 km). Geographic locations of industrial and populated large cities are indicated with white circles. DOI: https://doi.org/10.1525/elementa.394.f1

KORUS-AQ is an international air quality field study that was held in Korea, May–June 2016, which aimed to understand the factors controlling air quality across urban, rural, and coastal interfaces. During the campaign, extensive surface and airborne observations with high temporal resolutions were conducted using various instruments.

Measurements of reactive gaseous species onboard the NASA DC-8 aircraft enable a comprehensive analysis on the chemical formation and distribution of air pollutants. Airborne measurements used in this study include O_3, NO, NO_2, NO_y, OH, HO_2, and speciated VOCs. O_3, NO_x, and NO_y measurements were conducted using the NCAR NO–NO_y instrument which uses the chemiluminescence of NO by reaction with O_3 with a detection limit of 5–10 pptv/s (Ridley and Grahek, 1990). OH and HO_2 were measured using the Airborne Tropospheric Hydrogen Oxides Sensor (ATHOS) with a detection limit of 0.01 and 0.1 pptv (Brune et al., 1995).

Speciated VOCs including alkanes, alkenes, and aromatic hydrocarbons were collected in Whole Air Samples (WAS) and identified by laboratory analysis using gas chromatography with flame ionization detection, electron capture detection, and mass spectrometric detection. The detection limits for the VOCs are 2–3 pptv (https://airbornescience.nasa.gov/instrument/WAS_UCI). Isoprene, acetaldehyde (CH_3CHO), and formaldehyde (HCHO) measurements were also conducted using the Proton-Transfer-Reaction Time-of-Flight Mass Spectrometer (PTR-ToF-MS) (Müller et al., 2014) and the Compact Atmospheric Multispecies Spectrometer (CAMS) (Richter et al., 2015).

All research flights during the campaign landed and returned back to the air base at 16 LST (Local Standard Time), and O_3 observations showed highest values in the planetary boundary layer (PBL) during 13–16 LST. In order to focus on O_3 and its production characteristics, we used 60 second averaged DC-8 observations for cases where the plane flew over inland areas or near the coast with an altitude below 1.5 km during the photochemically active hours, 13–16 LST, in our analysis.

2.2 O_3 production efficiency (OPE) during KORUS-AQ

The production of O_3 varies nonlinearly with VOCs and NO_x concentrations (Lin et al., 1988). The OPE, which is an effective metric to examine the nonlinearity of O_3 production (Lin et al., 1988), is defined as the number of O_3 molecules produced per NO_x molecules consumed, P_{O_3}/L_{NO_x}, assuming a steady state for NO_x. Values are typically high (>10) in a clean rural region and low (<5) in a polluted urban region (Kleinman et al., 2002). In this study, we use this metric to understand the characteristics of O_3 formation in Korea.

Several observation-based studies used the regression slopes of the observed concentrations of O_3 versus NO_x oxidation products ($NO_z = NO_y - NO_x$) to obtain the OPE, and reported values ranging from 2 to 12, where the lowest values were observed in plumes with high NO_x conditions (Zaveri et al., 2003). However, this approach may lead to an ambiguous interpretation because observations contain air parcels with different photochemical histories and ages (Trainer et al., 2000). Furthermore, the magnitude of NO_z mixing ratios may differ depending on reactive nitrogen species that are included in defining NO_y (NO_x, PANs, HONO, HNO_3, NO_3, N_2O_5, organic nitrates, particulate nitrate, etc.). To avoid such issues, we explicitly calculate the instantaneous formation (F_{O_3}), destruction (D_{O_3}), net production rates of O_3 ($P_{O_3} = F_{O_3} - D_{O_3}$) and the loss rate of NO_x (L_{NO_x}) using equations (1–4) below in 3-D chemical transport simulations that we discuss in detail in section 2.3.

Equation (1) describes the daytime O_3 formation starting with the reaction of NO with the hydroperoxy radical (HO_2) and organic peroxy radicals (RO_2) to produce NO_2. Equation (2) represents the O_3 destruction rate, which includes the photolysis (followed by the reaction of $O(^1D)$ with H_2O) and the reaction of O_3 with HO_2, OH, VOCs (alkenes) and NO (followed by the reaction of NO_2 with OH). NO_x loss rate is calculated by equation (4), where NO_2 is oxidized by OH to produce HNO_3, which is scavenged by wet or dry deposition (Finlayson-Pitts and Pitts Jr, 2000).

$$F_{O_3} = k_{NO+HO_2}[NO][HO_2] + \sum_i k_{NO+RO_{2_i}}[NO][RO_{2_i}] \quad (1)$$

$$D_{O_3} = k_{O(^1D)+H_2O}[O(^1D)][H_2O] + k_{O_3+HO_2}[O_3][HO_2] + k_{O_3+OH}[O_3][OH] + \sum_i k_{O_3+VOC_i}[O_3][VOC_i] + k_{NO_2+OH}[NO_2][OH] \quad (2)$$

$$P_{O_3} = F_{O_3} - D_{O_3} \quad (3)$$

$$L_{NO_x} = k_{NO_2+OH}[NO_2][OH] \quad (4)$$

Instantaneous OPE is the rate of net O_3 production per the rate of NO_x loss, which can be obtained using equation (5).

$$OPE = P_{O_3}/L_{NO_x} \quad (5)$$

Time-dependent observation-constrained 0-D photochemical box modeling was conducted by the NASA Langley Research Center (LaRC) to simulate the oxidation and photochemical processes during KORUS-AQ. Model inputs derived from 1 second-merged DC-8 measurements of temperature, pressure, photolysis rates, O_3, CO, NO, H_2O_2, CH_3OOH, HNO_3, PAN, HCHO, and VOCs were used as constraints to calculate diurnal steady state concentrations of radical species. Using a customized chemical mechanism with reaction rates based on NASA JPL 2012 (https://jpldataeval.jpl.nasa.gov/index.html) and IUPAC 2006 recommendations, concentrations of NO_2, OH, HO_2 and RO_2 were simulated (Crawford et al., 1999; Schroeder et al., 2017). The model also calculated instantaneous production and loss rates of O_3 and NO_x, as described in equations (1–4). The box model calculations include dry deposition loss, and rainout loss based on Logan et al. (1981), but do not include any heterogeneous chemistry and convection. A full list of detailed chemical mechanisms used in the box model can be found in the supporting information of Schroeder et al. (2017).

Using the box model results and DC-8 measurements, instantaneous F_{O_3}, D_{O_3}, net P_{O_3}, and L_{NO_x} rates were calculated along the DC-8 flight track. Box model predictions

of NO_2, OH, and peroxy radicals are in good agreements with observations (Figure S1), and are further discussed in (Schroeder et al., in prep.). Therefore, we assume that the observation-constrained box model represents the true atmosphere and we use the box-model calculated OPE values to evaluate 3-D model simulations.

2.3 GEOS-Chem Chemical Transport Model

We use a 3-D global chemical transport model (GEOS-Chem v10-01) (Bey et al., 2001) and its nested configuration to simulate gas and aerosol species in Korea during the campaign. The model is driven by GEOS-FP (Forward Processing) assimilated meteorology provided by the GMAO at NASA Goddard Space Flight Center. The nested model covers the East Asian domain (70°E–140°E, 15°N–55°N) with a horizontal resolution of 0.25° × 0.3125° and 47 vertical layers. Boundary conditions are provided from a global simulation with 2° × 2.5° horizontal resolution. A one-month spin-up was conducted for both the global and nested simulations.

We update the default NO_x-O_x-Hydrocarbon-Aerosol mechanism to extend gas phase aromatic chemistry from that of Henze et al. (2008). The default mechanism includes abbreviated aromatic (benzene, toluene, xylene) oxidation chemistry, which does not fully represent the chemistry in Korea. One of important findings during the KORUS-AQ campaign is that aromatic species mixing ratios, especially toluene, are particularly high in Korea (NIER and NASA, 2017). This is also consistent with a recent observation-based study, which reported that toluene and xylenes are the most abundant aromatic hydrocarbons in Seoul (Khan et al., 2018), emphasizing the role of these reactive compounds in NO_x-O_x-VOC chemistry. Based on Porter et al. (2017), we include 7 additional intermediate species and corresponding gas phase kinetic and photolysis reactions in the model to simulate more explicit aromatic chemistry. A detailed list of additional mechanisms and species are summarized in Tables S2 and S3.

We use anthropogenic emissions of CO, NO_x, SO_2, NH_3, and VOCs for East Asia from the KORUS v2.0 inventory, developed by Konkuk University (Jang et al., 2019), who updated the inventory from its' previous version, using detailed regional segregation, GIS data, and 2015 control policies for Korea. Monthly emissions for South Korea were estimated by projecting the 2012 Korean national emissions inventory (Clean Air Policy Support System) with 3-year growth factors. Emissions from other countries including China and North Korea were from the NIER/KU-CREATE inventory (Woo et al., 2012). The anthropogenic emissions of CO, NO_x, SO_2, NH_3, and VOCs in South Korea are 941, 1000, 351, 286, and 1023 Gg/yr, respectively. Biomass burning emissions are taken from the daily GFED4 (Global Fire Emissions Database 4) inventory (R. van der Werf et al., 2010) and biogenic emissions are calculated by MEGAN (Model of Emissions of Gases and Aerosols from Nature) v2.1 (Guenther et al., 2012).

We conduct several model simulations including the baseline and sensitivity simulations which are summarized in **Table 1**. The first is conducted using GEOS-Chem v10-01 with anthropogenic and biogenic emissions discussed above. The latter are done using models with several updates and perturbations including updated aromatic chemistry, constrained PBL heights, and different anthropogenic NO_x emissions in the peninsula to examine the sensitivity of simulated O_3 and its characteristics. All the simulations are run for April 1st to June 10th, 2016 and we focus our analysis on the results for 20 research flights during the campaign. For a comparison of the simulations against airborne observations, we archive model results every minute for grid boxes corresponding to the 60 second averaged DC-8 flight tracks. Therefore, all the simulated and observed concentrations used in our analysis below are temporally and spatially coherent.

3. Effect of aromatic chemistry on simulated O_3 production

We first evaluate the baseline model (BASE) performance by comparing observed and simulated O_3 mixing ratios during the campaign. **Figure 1** shows the spatial distribution of observed and simulated mean O_3 mixing ratios averaged for 13–16 LST of the campaign below 1.5 km along the DC-8 flight track. The model generally captures the observed spatial distributions, i.e., high in urban areas and low in rural areas, but fails to capture the magnitude of measurements.

Figure 2 shows scatter-plot comparisons of the observed and simulated O_3 and NO_x mixing ratios during the campaign. The BASE model significantly underestimates O_3 and NO_x although no significant low biases are shown for reactive VOCs (Figure S2). We find that the update of aromatic chemistry in the model (AROM) substantially increases O_3 mixing ratios, which are in better agreements with the observations relative to those of the BASE model. This increase in O_3 production mainly results from more NO to NO_2 conversion driven by aromatic VOCs oxidation, especially by toluene and xylene, which show decreases with the update in the model. As a result, we find a large low bias of simulated NO_x levels in the AROM model. This

Table 1: Summary of the model (GEOS-Chem) simulations conducted in this study. DOI: https://doi.org/10.1525/elementa.394.t1

Model name	Chemistry	PBL height	Emissions
BASE	Default	Default	Default
AROM	Updated aromatic chemistry	Default	Default
PBL	Updated aromatic chemistry	Scaled PBL height	Default
PBL+NO_x	Updated aromatic chemistry	Scaled PBL height	50% increased NO_x

is also associated with increased formation of organic nitrates and PAN (Figure S2), which are important NO_x reservoirs produced during the oxidation of VOCs. Despite the decrease in NO_x mixing ratios, we find that the chemistry update effectively converts NO_x to organic nitrates, resulting in better agreements with observations.

We compare the instantaneous O_3 formation, O_3 destruction, and NO_x loss rates from the model as calculated using equations (1–4) with results from the observation-constrained box model described in section 2.2. Each term comprises the OPE and mean values averaged during the campaign are shown in **Figure 3**.

The O_3 formation rate, F_{O_3}, is calculated as the sum of the reaction rates of peroxy radicals and NO. Compared to the BASE simulation, updated aromatic chemistry increases both "HO_2+NO" and "RO_2+NO" terms but still underestimates F_{O_3} compared to the box model. Figure S1 shows that RO_2 is overestimated and HO_2 is underestimated in GEOS-Chem. Therefore, NO_x underestimation appears to be the main cause of the low formation rates compared to the box model.

While the O_3 destruction rate, D_{O_3}, is also underestimated in GEOS-Chem, O_3 losses by the "O_3+HO_2" and "NO_2+OH" reactions show largest discrepancies between the two models (**Figure 3 (b)**). An O_3 destruction increase by the "O_3+HO_2" reaction in the AROM model is associated with the increase in HO_2 mixing ratios. Despite the increase in the AROM model, the "O_3+HO_2" term is still smaller in GEOS-Chem than that of the box model, which can be explained by the underestimation of O_3 and HO_2 mixing ratios (Figure S1). The overestimation of >C3 alkenes (Figure S2) causes the overestimation of the "O_3+VOCs" term. The "NO_2+OH" contribution, which represents an O_3 loss by the reaction with NO, does not show a significant change from the BASE model to the AROM model. In both model runs, the underestimation of NO_x shown in **Figure 2** is the main contributor to the underestimation of O_3 loss rates by the "NO_2+OH" reaction relative to the box model result.

The difference between F_{O_3} and D_{O_3} is the net O_3 production rate, which is shown in **Figure 3 (c)**. Updated aromatic chemistry increases the simulated net O_3 production and NO_x loss rates in GEOS-Chem by 37% and 22%. This explains the increase in O_3 and the decrease in NO_x mixing ratios shown in **Figure 2**. However, because NO_x is highly underestimated in GEOS-Chem, L_{NO_x} underestimation still exists.

NO_x underestimation may imply either the underestimation of emissions or model uncertainties in chemical, thermodynamic or physical processes such as NO_x recycling, NO_y partitioning or boundary layer mixing (Bertram et al., 2013), which will be further discussed in section 4.2.

4. Sensitivity of the model to PBL height and NO_x emissions

4.1 Model sensitivity to PBL height

The PBL height (i.e., mixing layer height) is a key factor that controls the vertical mixing and surface concentrations of pollutants (Tong et al., 2011). In this section, we examine the sensitivity of the model to changes in PBL heights, which are constrained by the lidar observations. In addition, we conduct model sensitivity analyses to anthropogenic NO_x emission changes and their effects on the simulated O_3 formation.

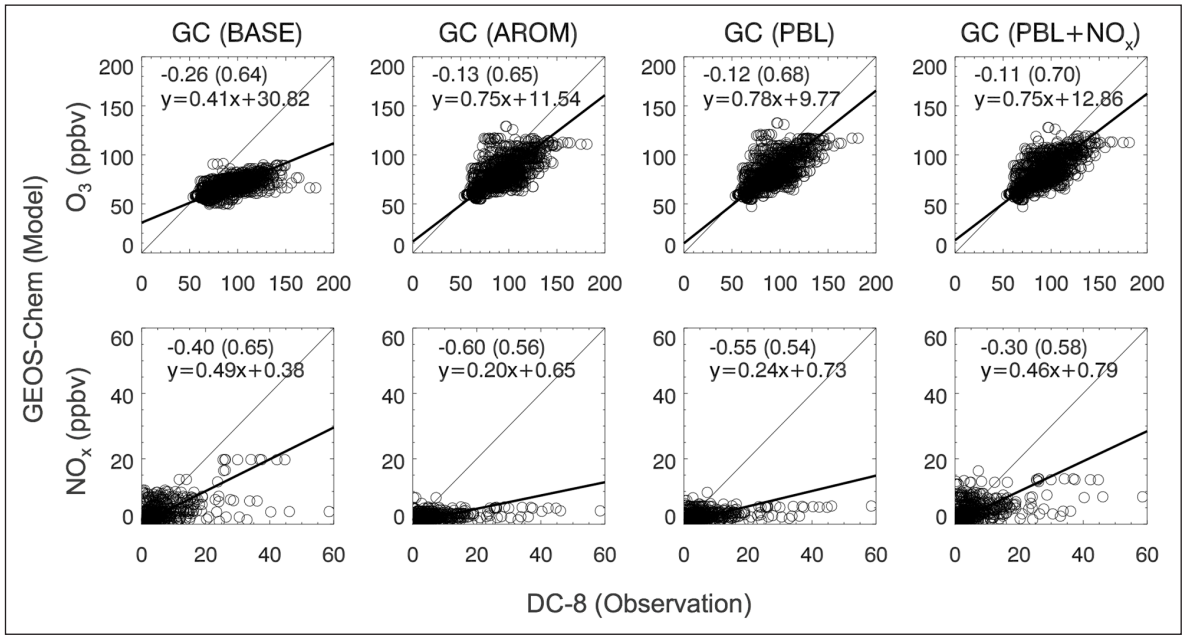

Figure 2: Scatter-plot comparisons of observed and simulated O_3 and NO_x. Simulated (GEOS-Chem) versus observed (DC-8) concentrations of O_3 and NO_x below 1.5 km during 13–16 LST. For all panels the axes indicate DC-8 observations (x-axis) and simulations (y-axis). The NMB, Pearson correlation coefficient (in parentheses) and the regression equation are stated in the upper corners. The normalized mean bias (NMB) between the model and observation is calculated as $NMB = \frac{\sum_{i=1}^{N}(M_i - O_i)}{\sum_{i=1}^{N} O_i}$, where N denotes the total number of data points, M indicates the model value and O indicates the observed value. DOI: https://doi.org/10.1525/elementa.394.f2

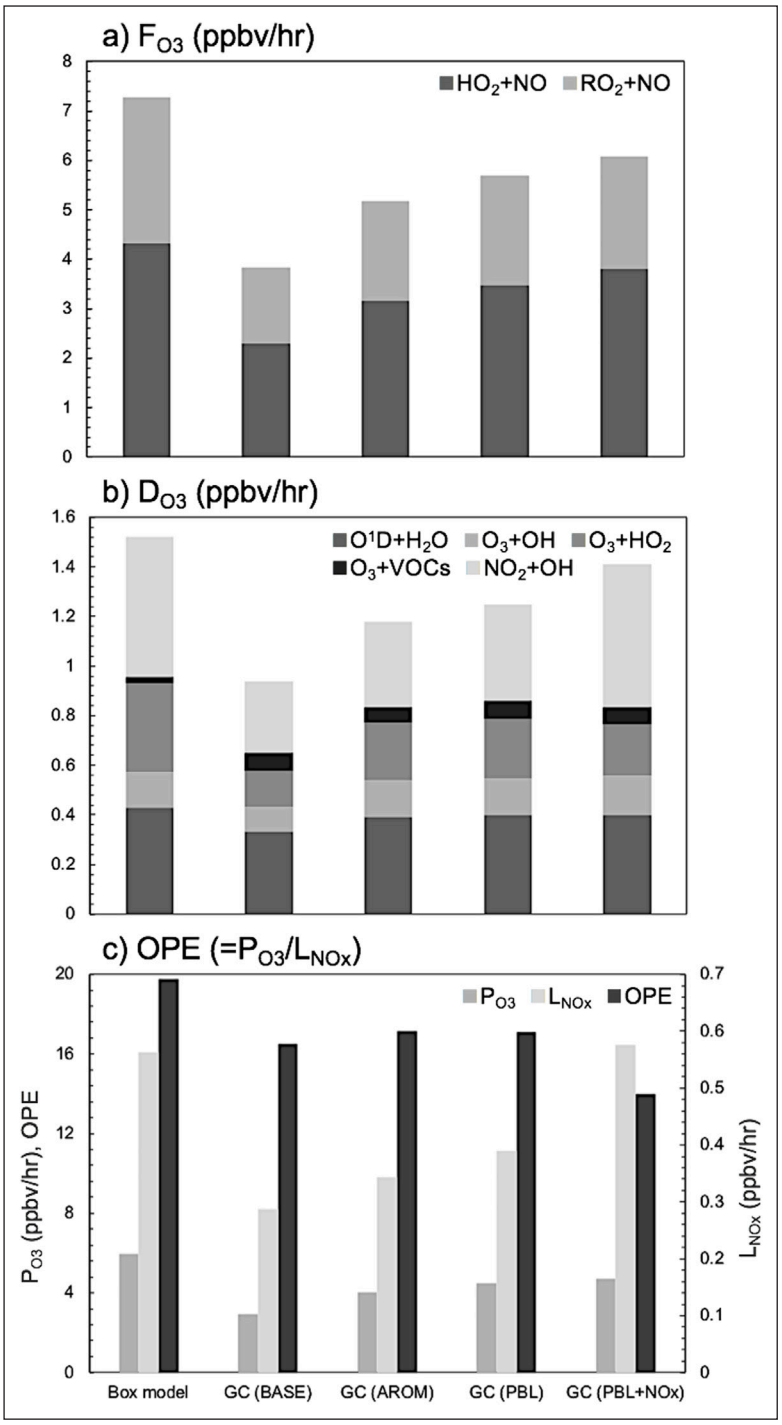

Figure 3: Comparison of simulated F_{O_3}, D_{O_3}, and OPE. Average **a)** O_3 formation rate, **b)** O_3 destruction rate, and **c)** OPE during the campaign. Different shades indicate each term that comprises the total quantities. DOI: https://doi.org/10.1525/elementa.394.f3

Previous studies have reported that air quality models generally overestimate the daytime evolution of the PBL heights compared to lidar or ceilometer measurements (Haman et al., 2014; Scarino et al., 2014). Scarino et al. (2014) described that the discrepancy could be due to model resolutions, which are generally too coarse to account for the sub-grid scale variation of terrain heights, while Haman et al. (2014) explained that the modeled PBL showed too rapid growth driven by faster wind speeds than observations.

PBL heights are commonly observed by the inversion of the potential temperature profile or as a peak in low level wind (Grossman and Gamage, 1995; Holzworth, 1964). Lidar backscatter profiles are also widely used to examine the structure and variability of PBL heights (Brooks, 2003). During the campaign, PBL heights were measured at Seoul National University (SNU, 126.95°E, 37.46°N) using lidar observations with the retrieval algorithm introduced by Brooks (2003) and are used for the model evaluation in this study. **Figure 4** compares simulated versus observed hourly PBL heights at SNU averaged for the campaign and we find large discrepancies of up to a factor 1.3 during 13–15 LST in the model relative to the lidar-derived values.

The lidar-derived PBL height indicates the height of transition from a particle-rich layer near the surface to a cleaner layer aloft. Therefore, lidar-derived PBL heights are often higher than the meteorological transition heights during the nighttime when the residual layer and mixing layer coexist (Bravo-Aranda et al., 2017). Due to the residing or transported aerosol layer existing above 0.7–0.8 km, there could be few cases where the retrieved nighttime PBL heights might be overestimated. However, these cases did not affect the average diurnal profile of the whole period and even for our analysis, which mainly focuses on the daytime.

In order to test the effect of boundary layer mixing within the PBL in the model, we used average diurnal profiles of the PBL to calculate hourly scale factors based on the discrepancy between the model and lidar observations at SNU. Although the hourly scale factors are based on model evaluation at only one grid box, the same scale factors were applied to other grid boxes for the rest of South Korea. The scaled PBL heights are lower in the daytime and higher in the nighttime compared to the PBL heights in the baseline model, reducing the gap between the model and lidar observations as shown in **Figure 4**.

Constraining the daytime PBL heights based on the lidar-derived observations increases O_3 and its precursors mixing ratios in the model. Correspondingly, both the P_{O_3} and L_{NO_x} terms increase and show better agreements with the box model results (**Figure 3**).

Figure 5 shows the mean vertical profiles of NO_x mixing ratios averaged in urban and rural regions, respectively, and over the whole Korea. Urban regions include major metropolitan cities such as the SMA, Busan, Daegu and Ulsan (indicated in **Figure 1**). The AROM model fails to capture the vertical gradient shown in DC-8 observations

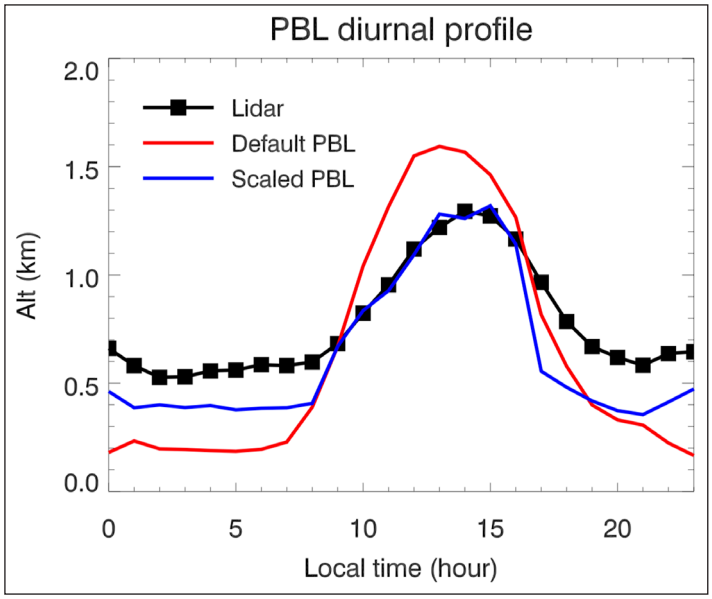

Figure 4: Diurnal profiles of observed (lidar) and simulated PBL heights. Mean diurnal profiles of modeled (colored) and lidar-derived (black) PBL heights at Seoul National University. Red and blue solid lines each indicate the modeled PBL height with no modification and the constrained PBL height using hourly scale factors, respectively. DOI: https://doi.org/10.1525/elementa.394.f4

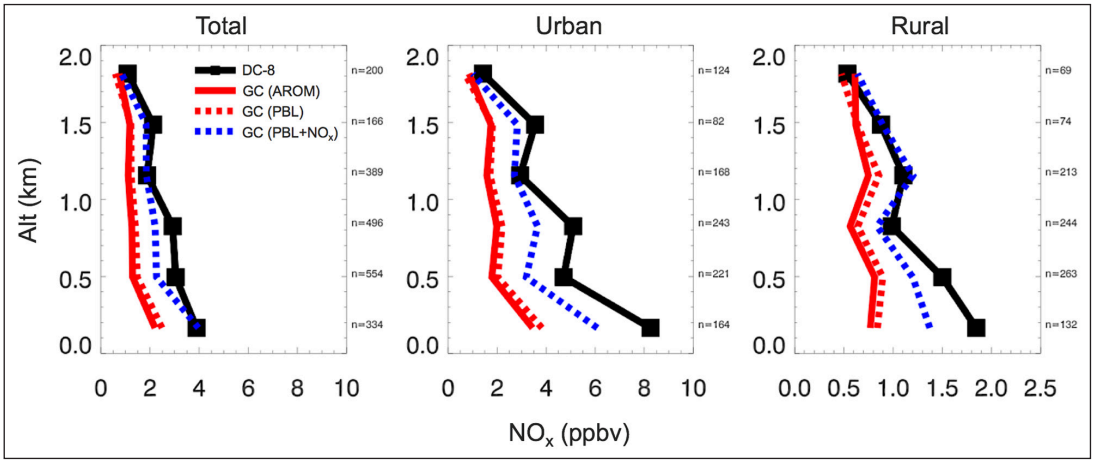

Figure 5: Vertical profiles of observed and simulated NO_x. Mean vertical profiles of observed (black) and simulated NO_x mixings. Colored lines indicate simulated NO_x profiles, and dotted lines indicate results using scaled PBL heights. The number of averaged data is denoted on the left sides of each panel. DOI: https://doi.org/10.1525/elementa.394.f5

and shows that model underestimation is mostly located near the surface. Although the simulated NO_x mixing ratios show a 5% increase when the PBL height is scaled based on the observation (**Figure 2**), this is not large enough to reduce the discrepancy in the model. Moreover, NO_x levels are still significantly underestimated in the model for both urban and rural areas.

4.2 Model sensitivity to local NO_x emissions

Based on the model underestimation of surface NO_x levels we increased NO_x emissions in South Korea by 50%. **Figure 5** shows that when the emissions are increased, simulated NO_x mixing ratios are significantly enhanced and become much closer to the observations especially above 1 km. It appears that the model still underestimates observed NO_x levels at the surface and the further increase in NO_x emissions could decrease the simulated discrepancy, but our analysis of total reactive nitrogen (NO_y) and O_3 production characteristics below does not allow for this.

We further separated the analyses into four different periods (dynamic weather, stagnant, extreme pollution, blocking pattern) based on synoptic weather conditions during the campaign (Peterson et al., in review) to separate the effects of transboundary transport versus local emissions on ambient NO_x and NO_y levels in Korea. Figure S3 shows mean sea level pressures (SLP) and wind vectors in the model for each period. Unlike the dynamic weather period, the influence of local emissions was dominant for the Korean peninsula during the stagnant period due to weak wind speeds and inefficient mixing associated with a persistent high pressure system located over East Asia. We found the highest levels of surface pollutants such as O_3 and $PM_{2.5}$ during the extreme pollution period, exceeding the Korea air quality standards (NIER and NASA, 2017). During this period, due to weakening of the polar jet stream over Central Asia and the weaker vertical motion, direct transport from China accompanied with the westerlies was important, causing high levels of pollutants in surface air in Korea (Peterson et al., in review).

Figure 6 shows that during the dynamic weather and extreme pollution periods, modeled NO_x and NO_y levels are higher than observations in all four sensitivity simulations. In contrast, during the stagnant and blocking pattern periods with dominant effects of local emissions, model results with increased NO_x emissions show better agreement with observations, especially in urban areas. This indicates that local NO_x sources are likely underestimated in the inventory.

Model results from the PBL+NO_x model show increases in NO_x mixing ratios as well as L_{NO_x} (**Figures 2** and **3**). We find model improvements in the regression slope of L_{NO_x} (0.83) and correlation (0.58) with the box model relative to other simulations. Model performance in simulating O_3 also shows improvements in terms of both the normalized mean bias (−11%) and correlation (0.70) with observations.

Despite the 50% increase in NO_x emissions, **Figure 2** shows that the model still underestimates NO_x mixing ratios compared to the observations. Recent studies suggest that additional mechanisms such as nitryl chloride chemistry (Sarwar et al., 2012) and nitrate photolysis (Ye et al., 2017) can improve the simulations of nitrogen chemistry in air quality models. Choi et al. (2019) implemented particulate nitrate photolysis in GEOS-Chem using parameters from Ye et al. (2017) and found a significant improvement in particulate nitrate, HONO, and NO_x simulations. Our study focuses on constraining NO_x emissions based on the model evaluation regarding O_3 production characteristics, but there still remains a limitation. A further study is necessary to account for the additional NO_x chemistry that is currently absent in the model.

Figure 7 shows the VOCs and NO_x dependency of instantaneous OPEs calculated in the box model and GEOS-Chem. VOCs include ethane, propane, large alkanes

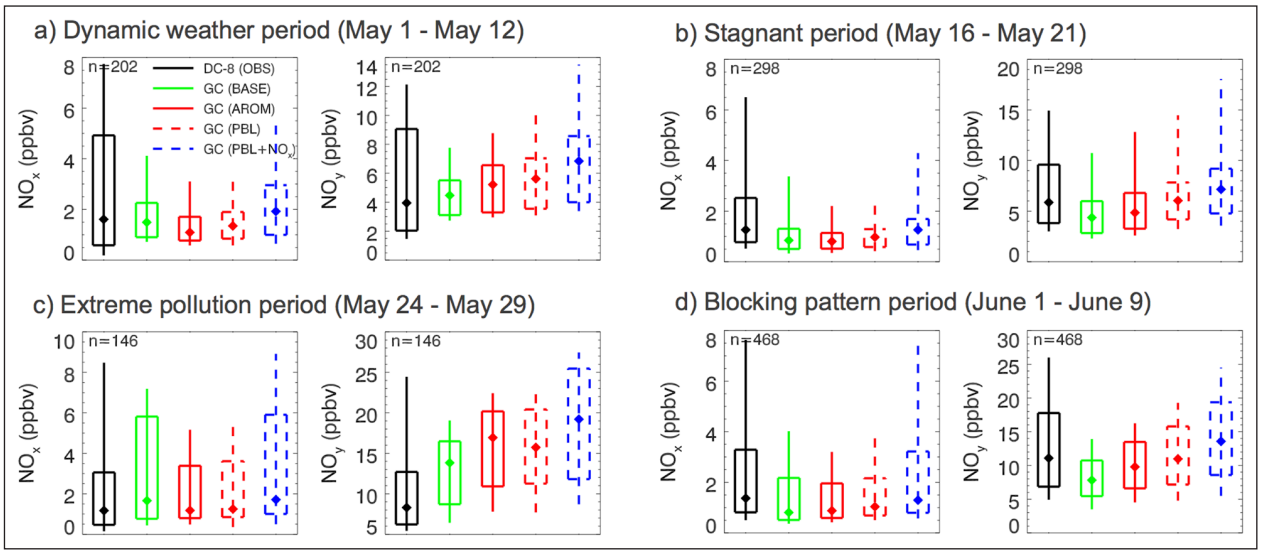

Figure 6: Comparison of observed and simulated NO_x and NO_y during four different synoptic weather patterns in East Asia. Box-plot comparison of observed and simulated NO_x and NO_y below 1.5 km during 13–16 LST for each period defined in Figure S3. The bars and lines each indicate the interquartile range and the 10–90th percentiles, respectively, and the diamond indicates the median value. DOI: https://doi.org/10.1525/elementa.394.f6

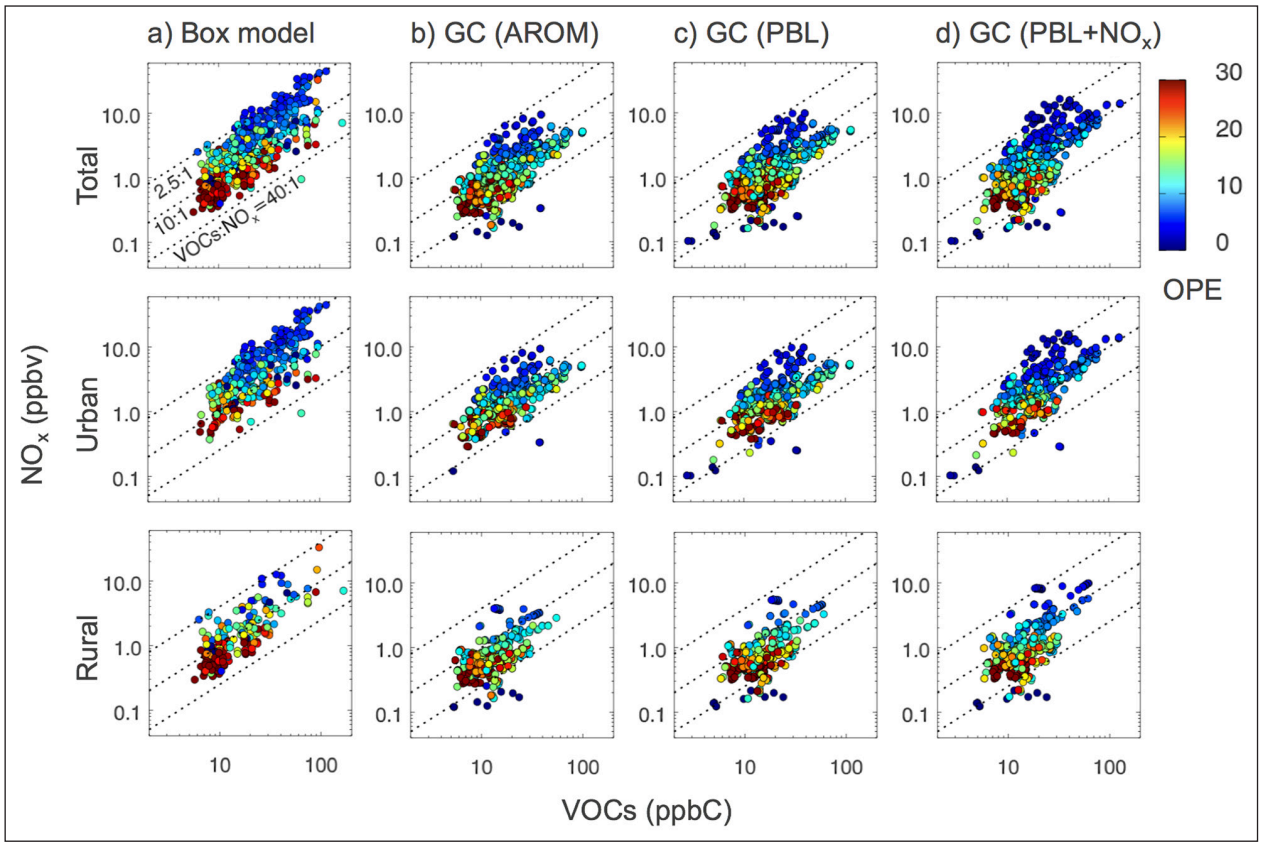

Figure 7: VOCs and NO_x dependency of simulated OPEs. VOCs and NO_x dependence of instantaneous OPEs calculated from the box model and GEOS-Chem. Data points are color-coded by OPE values and each row indicates total Korea, urban, and rural areas. Dashed lines indicate three different VOC to NO_x ratios (VOC/NO_x), 40, 10, 2.5, from bottom to top. DOI: https://doi.org/10.1525/elementa.394.f7

(>C4), large alkenes (>C3), benzene, toluene, xylene, isoprene, monoterpenes, methyl ethyl ketone (MEK), and acetaldehyde. In the observation-constrained box model, low OPE values are shown above the 10:1 line, indicating that urban areas in Korea are VOC-limited. Rural areas tend to have higher OPE values that are located below the 10:1 line. General characteristics of the observed OPE dependency on precursor concentrations also appear in GEOS-Chem. However, due to the underestimation of NO_x, GEOS-Chem results are slightly shifted to a NO_x-limited regime compared to the box model.

The simulated results with scaled PBL heights shown in **Figure 7 (c)** and **(d)** show larger scatters compared to **Figure 7 (b)**, elongating the location of the points diagonally, which is caused by the lower PBL height. Decreased PBL heights tend to decrease species mixing ratios in upper levels (~1.5 km) compared to the base PBL simulation. This results in decreases of NO_x and VOCs mixing ratios around 1.5 km, which correspond to the data points located in the lower left corners in **Figure 7 (c)** and **(d)**. The overall comparison of GEOS-Chem to the observation-constrained box model indicates that the PBL+NO_x model (**Figure 7 (d)**) shows the best performance in reproducing the observed O_3 production regimes in Korea.

Considering the underestimation of aromatic VOCs in GEOS-Chem (Figure S2), we additionally doubled toluene emissions to investigate the sensitivity of OPE to aromatic VOCs emissions. Although we see a slight increase in the OPE, a negligible change is found compared to **Figure 7 (d)** and therefore we conclude that the OPE is more sensitive to NO_x emissions than aromatic VOCs emissions in Korea.

5. Sensitivity of OPE to emission changes in Korea

The Korean government aims to achieve a 30% reduction of domestic emissions (from industries, powerplants, diesel cars, etc.) by 2022 as part of the $PM_{2.5}$ concentrations reduction policy (Ministry of Environment, 2017). However, this emission change may also have a profound impact on O_3 levels in Korea. To estimate the effect of regulation we conduct sensitivity simulations and investigate the change in O_3 and the OPE with respect to emissions control in the future. Using our best-performing model (PBL+NO_x) as the base run, we compare the results with 30% decreased NO_x and anthropogenic VOCs emissions over Korea.

Figure 8 shows the spatial distributions of simulated ground level OPEs during May 2016. Typical features of the OPE such as high in clean regions and low in polluted regions are well captured. In the base run, we find maximum OPE of ~20 along the mountain range located in the middle, where biogenic VOCs emissions are dominant, and minimum values in high NO_x regions such as the SMA. In both the sensitivity runs the reduction in emissions increases the OPE throughout the country. When only NO_x emissions are controlled, the OPE reaches up

to 30 in rural regions, indicating that these NO_x-limited regions become much more efficient in producing O_3 with the same amount of NO_x. With NO_x and VOCs emissions controlled together, the OPE increase is less prominent, showing a maximum of ~25.

Figure 9 shows the OPE, O_3 mixing ratios, and NO_x lifetime changes as a response to the emissions control. We find that the decrease in precursor emissions does not have a linear impact on O_3. In rural regions where NO_x plays the major role in O_3 production, O_3 mixing ratios decrease and the NO_x lifetime increases due to less oxidation by OH (i.e., decrease in NO_x loss). In urban (e.g., Seoul, Busan) and industrial areas (e.g., Daesan, Pohang, Ulsan, Yeosu) which are under VOC-limited conditions, O_3 increases (~6

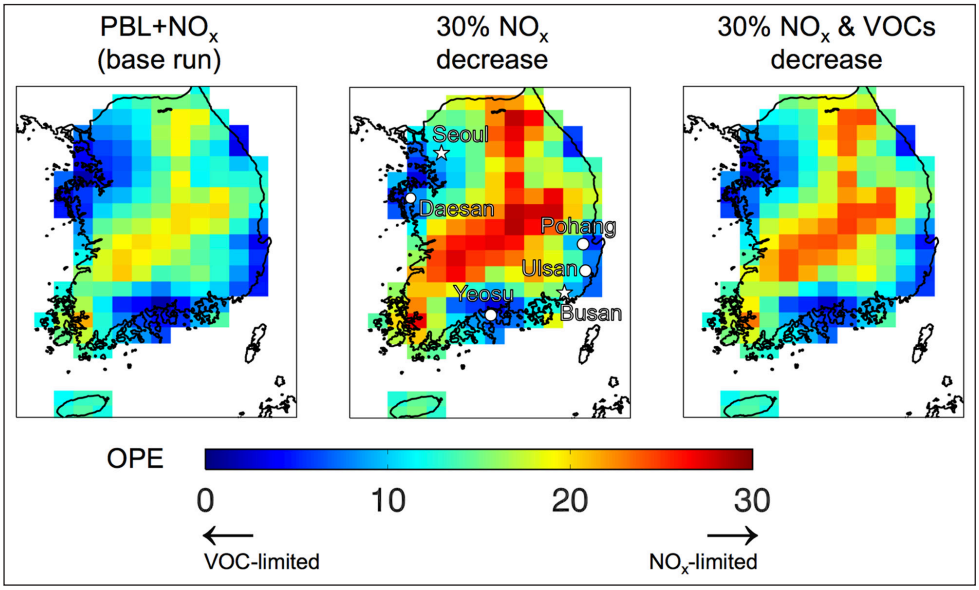

Figure 8: Spatial distributions of simulated OPEs and responses to emission change. Spatial distributions of simulated OPE at surface level and responses to NO_x and VOCs emission changes in South Korea. All simulations are run using the same configuration as the PBL+NO_x model. Major metropolitan and industrial areas are indicated with stars and circles, respectively. DOI: https://doi.org/10.1525/elementa.394.f8

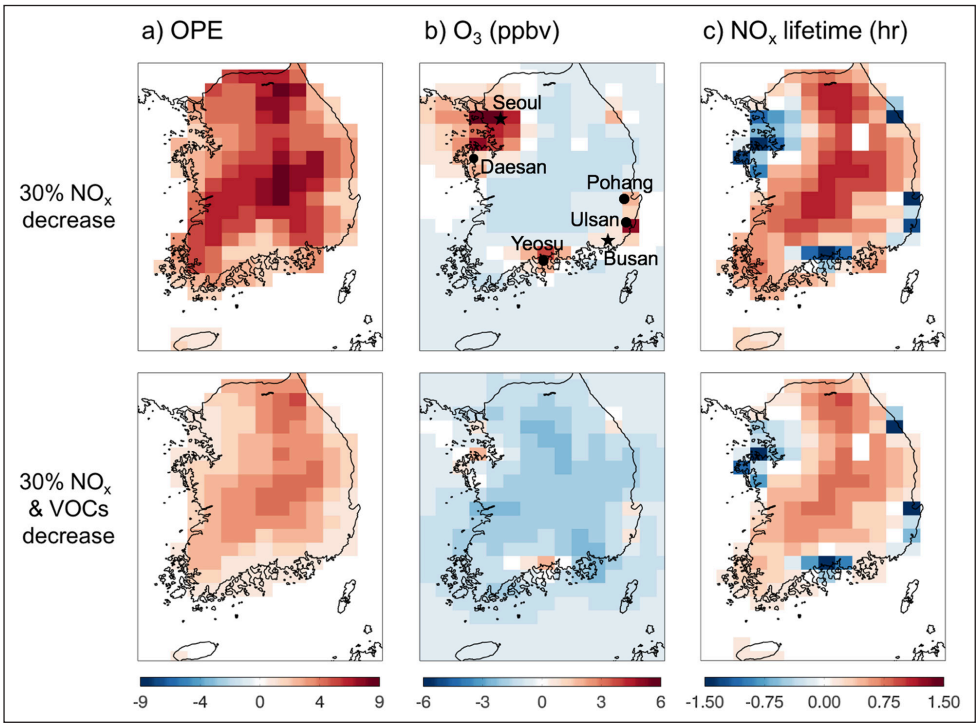

Figure 9: Spatial distributions of simulated OPE, O_3, and NO_x lifetime changes. Spatial distributions of changes (modified emissions run minus base run) in simulated surface a) OPE, b) O_3 levels, and c) NO_x lifetime as a response to emission changes. Major metropolitan and industrial areas are indicated with stars and circles, respectively. DOI: https://doi.org/10.1525/elementa.394.f9

ppbv) and NO_x lifetimes show noticeable decreases as a result of NO_x reductions. With concurrent VOCs reductions, although there are some signals of O_3 increase in industrial areas the magnitudes are significantly smaller than those without VOCs reductions, and O_3 decreases are shown in major metropolitan areas.

Table 2 summarizes the changes of O_3 production characteristics that appear in different regimes in the sensitivity simulations. In VOC-limited regions (i.e., urban and industrial), a decrease in NO_x emissions results in an increase in O_3 levels. Two contributing factors, an increase of the O_3 formation rate due to faster NO_x recycling (i.e., higher OPE) and a decrease of the O_3 destruction rate via NO_x titration result in an increase of O_3 mixing ratios. Despite the decrease in ambient NO_x mixing ratios (−36%), F_{O_3} shows an increase (+9%) due to the efficient HO_x–NO_x cycling. Because the decrease in L_{NO_x} (−19%) reflects the decrease of NO_x titration, we can imply that the impact of less titration is the predominant factor that causes the O_3 increase in these areas. With an additional VOCs reduction, the decrease of O_3 precursors results in a decrease of net production. On the other hand, NO_x titration is of less importance for O_3 levels in NO_x-limited regions. The 30% decrease in precursor emissions does not directly decrease O_3 mixing ratios by 30% because of the nonlinear chemistry. However, the simulation results show that the tendency of O_3 production follows the change in precursor emissions in rural areas.

6. Summary and Conclusions

An observation-constrained box model and a 3-D chemical transport model (GEOS-Chem), were used to obtain instantaneous O_3 production efficiencies ($OPE = P_{O_3}/L_{NO_x}$) in Korea during May–June 2016. The sensitivity of simulated OPE was tested to examine the effect of aromatic chemistry and anthropogenic NO_x and VOCs emissions on O_3 production.

Table 2: Relative differences[a] of O_3, NO_x, O_3 production, and destruction terms with respect to the base run. DOI: https://doi.org/10.1525/elementa.394.t2

	Urban & Industrial areas		Rural areas	
	30% NO_x decrease	30% NO_x & VOCs decrease	30% NO_x decrease	30% NO_x & VOCs decrease
O_3	+3%	0%	−1%	−2%
NO_x	−36%	−36%	−34%	−28%
F_{O_3}	+9%	−9%	−14%	−17%
D_{O_3}	−9%	−13%	−12%	−12%
P_{O_3}	+13%	−8%	−15%	−18%
L_{NO_x}	−19%	−21%	−36%	−30%
OPE	+40%	+18%	+32%	+17%

[a] The relative difference between the base and sensitivity run is calculated as $Difference = \frac{S-B}{B} \times 100$ (%), where S indicates the sensitivity run and B indicates the base run value.

Based on box model calculations, O_3 production in urban areas in Korea showed VOC-limited characteristics and OPE values were less than 10 in general. In rural areas, O_3 production tended to be more NO_x-limited and OPE values were higher than 20. Average OPE values over Korea calculated from the box model and GEOS-Chem with default chemistry and updated aromatic chemistry were 19.8, 16.5, and 17.2, respectively.

Our model evaluation showed that aromatic chemistry itself can increase the average net O_3 production in Korea by 37%. The overestimation of the daytime PBL height in the model was found to be responsible for ~10% decrease in both the net O_3 production and NO_x loss rates. The vertical distribution of simulated and observed NO_x mixing ratios and comparison of O_3 production regimes in different model runs clearly showed the underestimation of NO_x was mainly caused by the underestimation of NO_x emissions in the current inventory. Increasing 50% of NO_x emissions in the model improved model performance in reproducing the observed O_3 production and NO_x loss rates.

Sensitivity tests showed that the 30% decrease in anthropogenic emissions increases the OPE throughout the country, making rural regions ~2 times more efficient in producing O_3. However, without the VOCs emissions reduction, the NO_x emissions reduction alone can result in significant increases in O_3 levels in both urban and industrial regions. This implies the importance of concurrent emission reductions for both NO_x and VOCs in order to effectively reduce O_3 levels in Korea.

Data Accessibility Statement

Observational data from KORUS-AQ used in this study can be downloaded in the International Consortium for Atmospheric Research on Transport and Transformation (ICARTT) format through the data archive website (https://www-air.larc.nasa.gov/cgi-bin/ArcView/korusaq).

Supplemental files

The supplemental files for this article can be found as follows:

- **Figure S1.** Comparison of observed and simulated NO_2 and radical species. DOI: https://doi.org/10.1525/elementa.394.s1
- **Figure S2.** Comparison of observed and simulated organic nitrates, PAN, and speciated VOCs. DOI: https://doi.org/10.1525/elementa.394.s1
- **Figure S3.** Mean sea level pressures (SLP) and wind vectors in GEOS-Chem during four different synoptic weather patterns in East Asia. DOI: https://doi.org/10.1525/elementa.394.s1
- **Table S1.** Gas phase reactions of aromatic chemistry in GEOS-Chem based on Henze et al. (2008). DOI: https://doi.org/10.1525/elementa.394.s1
- **Table S2.** Gas phase reactions of aromatic chemistry added in GEOS-Chem based on Porter et al. (2017). DOI: https://doi.org/10.1525/elementa.394.s1
- **Table S3.** Aromatic species and reaction intermediates added in GEOS-Chem. DOI: https://doi.org/10.1525/elementa.394.s1

Acknowledgements

We thank all members of the KORUS-AQ team for their contributions during the field campaign and the agencies operating the measurements onboard DC-8. PTR-ToF-MS measurements aboard the NASA DC-8 during KORUS-AQ were supported by the Austrian Federal Ministry for Transport, Innovation and Technology (bmvit) through the Austrian Space Applications Programme (ASAP) of the Austrian Research Promotion Agency (FFG). The PTR-ToF-MS instrument team (P. Eichler, L. Kaser, T. Mikoviny, M. Müller) is acknowledged for their support with field work and data processing.

Funding information

This work was supported by the National Research Foundation of Korea (NRF) grant funded by the Korean government (MSIT) (No. 2018004494).

Competing interests

The authors have no competing interests to declare.

Author contributions

- Contributed to conception and design: YJO, RJP
- Contributed to acquisition of data: JRS, JHC, DRB, AJW, J-HW, S-WK, HY, AF, AW, WHB
- Contributed to analysis and interpretation of data: YJO, RJP, JRS, JHC
- Drafted and/or revised the article: YJO, RJP, JHC, S-WK
- Approved the submitted version for publication: RJP, JHC

References

Bertram, TH, Perring, AE, Wooldridge, PJ, Dibb, J, Avery, MA and **Cohen, RC.** 2013. On the export of reactive nitrogen from Asia: NO_x partitioning and effects on ozone. *Atmos Chem Phys* **13**(9): 4617–4630. DOI: https://doi.org/10.5194/acp-13-4617-2013

Bey, I, Jacob, DJ, Yantosca, RM, Logan, JA, Field, BD, Fiore, AM, Li, Q, Liu, HY, Mickley, LJ and **Schultz, MG.** 2001. Global modeling of tropospheric chemistry with assimilated meteorology: Model description and evaluation. *Journal of Geophysical Research: Atmospheres* **106**(D19): 23073–23095. DOI: https://doi.org/10.1029/2001JD000807

Bravo-Aranda, JA, de Arruda Moreira, G, Navas-Guzmán, F, Granados-Muñoz, MJ, Guerrero-Rascado, JL, Pozo-Vázquez, D, Arbizu-Barrena, C, Olmo Reyes, FJ, Mallet, M and **Alados Arboledas, L.** 2017. A new methodology for PBL height estimations based on lidar depolarization measurements: Analysis and comparison against MWR and WRF model-based results. *Atmos Chem Phys* **17**(11): 6839–6851. DOI: https://doi.org/10.5194/acp-17-6839-2017

Brooks, IM. 2003. Finding Boundary Layer Top: Application of a Wavelet Covariance Transform to Lidar Backscatter Profiles. *Journal of Atmospheric and Oceanic Technology* **20**(8): 1092–1105. DOI: https://doi.org/10.1175/1520-0426(2003)020<1092:FBLTAO>2.0.CO;2

Brune, WH, Stevens, PS and **Mather, JH.** 1995. Measuring OH and HO_2 in the Troposphere by Laser-Induced Fluorescence at Low Pressure. *Journal of the Atmospheric Sciences* **52**(19): 3328–3336. DOI: https://doi.org/10.1175/1520-0469(1995)052<3328:MOAHIT>2.0.CO;2

Chang, K-L, Petropavlovskikh, I, Copper, OR, Schultz, MG and **Tao, W.** 2017. Regional trend analysis of surface ozone observations from monitoring networks in eastern North America, Europe and East Asia. *Elem Sci Anth* **5**: 50. DOI: https://doi.org/10.1525/elementa.243

Choi, J, Park, RJ, Lee, H-M, Lee, S, Jo, DS, Jeong, JI, Henze, DK, Woo, J-H, Ban, S-J, Lee, M-D, Park, M-K, Shin, HJ, Cho, S, Peterson, D and **Song, C-K.** 2019. Impacts of local vs. trans-boundary emissions from different sectors on $PM_{2.5}$ exposure in South Korea during the KORUS-AQ campaign. *Atmospheric Environment* **203**: 196–205. DOI: https://doi.org/10.1016/j.atmosenv.2019.02.008

Crawford, J, Davis, D, Olson, J, Chen, G, Liu, S, Gregory, G, Barrick, J, Sachse, G, Sandholm, S, Heikes, B, Singh, H and **Blake, D.** 1999. Assessment of upper tropospheric HO_x sources over the tropical Pacific based on NASA GTE/PEM data: Net effect on HO_x and other photochemical parameters. *Journal of Geophysical Research: Atmospheres* **104**(D13): 16255–16273. DOI: https://doi.org/10.1029/1999JD900106

Finlayson-Pitts, BJ and **Pitts, JN, Jr.** 2000. CHAPTER 6 – Rates and Mechanisms of Gas-Phase Reactions in Irradiated Organic – NO_x – Air Mixtures. *Chemistry of the Upper and Lower Atmosphere*, 179–263. San Diego: Academic Press. DOI: https://doi.org/10.1016/B978-012257060-5/50008-3

Grossman, RL and **Gamage, N.** 1995. Moisture flux and mixing processes in the daytime continental convective boundary layer. *Journal of Geophysical Research: Atmospheres* **100**(D12): 25665–25674. DOI: https://doi.org/10.1029/95JD00853

Guenther, AB, Jiang, X, Heald, CL, Sakulyanontvittaya, T, Duhl, T, Emmons, LK and **Wang, X.** 2012. The Model of Emissions of Gases and Aerosols from Nature version 2.1 (MEGAN2.1): an extended and updated framework for modeling biogenic emissions. *Geoscientific Model Development* **5**(6): 1471–1492. DOI: https://doi.org/10.5194/gmd-5-1471-2012

Haman, CL, Couzo, E, Flynn, JH, Vizuete, W, Heffron, B and **Lefer, BL.** 2014. Relationship between boundary layer heights and growth rates with ground-level ozone in Houston, Texas. *Journal of Geophysical Research: Atmospheres* **119**(10): 6230–6245. DOI: https://doi.org/10.1002/2013JD020473

Han, Z, Sakurai, T, Ueda, H, Carmichael, GR, Streets, D, Hayami, H, Wang, Z, Holloway, T, Engardt, M, Hozumi, Y, Park, SU, Kajino, M, Sartelet, K, Fung, C, Bennet, C, Thongboonchoo, N, Tang, Y, Chang, A, Matsuda, K and **Amann, M.** 2008. MICS-Asia II: Model intercomparison and evaluation

of ozone and relevant species. *Atmospheric Environment* **42**(15): 3491–3509. DOI: https://doi.org/10.1016/j.atmosenv.2007.07.031

Henze, DK, Seinfeld, JH, Ng, NL, Kroll, JH, Fu, TM, Jacob, DJ and **Heald, CL.** 2008. Global modeling of secondary organic aerosol formation from aromatic hydrocarbons: High- vs. low-yield pathways. *Atmos Chem Phys* **8**(9): 2405–2420. DOI: https://doi.org/10.5194/acp-8-2405-2008

Holzworth, GC. 1964. Estimates of mean maxiumum mixing depths in the contigouous United States. *Monthly Weather Review* **92**(5): 235–242. DOI: https://doi.org/10.1175/1520-0493(1964)092<0235:EOMMMD>2.3.CO;2

Imhoff, RE, Valente, R, Meagher, JF and **Luria, M.** 1995. The production of O_3 in an urban plume: Airborne sampling of the Atlanta urban plume. *Atmospheric Environment* **29**(17): 2349–2358. DOI: https://doi.org/10.1016/1352-2310(94)00305-5

Jang, Y, Lee, Y, Kim, J, Kim, Y and **Woo, J-H.** 2019. Improvement China Point Source for Improving Bottom-Up Emission Inventory. *Asia-Pacific Journal of Atmospheric Sciences*. DOI: https://doi.org/10.1007/s13143-019-00115-y

Jeong, Y-M, Lee, S-H, Lee, H-W and **Jeon, W-B.** 2012. Numerical Study on the Process Analysis of Ozone Production due to Emissions Reduction over the Seoul Metropolitan Area. *Journal of Environmental Science International* **21**(3): 339–349. DOI: https://doi.org/10.5322/JES.2012.21.3.339

Jung, J, Lyu, Y, Lee M, Hwang, T, Lee, S and **Oh, S.** 2016. Impact of Siberian forest fires on the atmosphere over the Korean Peninsula during summer 2014. *Atmospheric Chemistry and Physics* **16**: 6757–6770. DOI: https://doi.org/10.5194/acp-16-6757-2016

Kang, Y-H, Oh, I, Jeong, J-H, Bang, J-H, Kim, Y-K, Kim, S, Kim, E, Hong, J-H and **Lee, D-G.** 2016. Comparison of CMAQ Ozone Simulations with Two Chemical Mechanisms (SAPRC99 and CB05) in the Seoul Metropolitan Region. *Journal of Environmental Science International* **25**(1): 85–97. DOI: https://doi.org/10.5322/JESI.2016.25.1.85

Khan, A, Szulejko, JE, Kim, K-H and **Brown, RJC.** 2018. Airborne volatile aromatic hydrocarbons at an urban monitoring station in Korea from 2013 to 2015. *Journal of Environmental Management* **209**: 525–538. DOI: https://doi.org/10.1016/j.jenvman.2017.12.055

Kim, J, Sung Ghim, Y, Han, J, Park, S-M, Shin, H-J, Sang-Bo Lee, S-B, Kim, J and **Lee, G.** 2018. Long-term Trend Analysis of Korean Air Quality and Its Implication to Current Air Quality Policy on Ozone and PM10. *Journal of Korean Society for Atmospheric Environment* **34**: 1–15. DOI: https://doi.org/10.5572/KOSAE.2018.34.1.001

Kim, MJ, Park, RJ, Ho, C-H, Woo, J-H, Choi, K-C, Song, C-K and **Lee, J-B.** 2015. Future ozone and oxidants change under the RCP scenarios. *Atmospheric Environment* **101**: 103–115. DOI: https://doi.org/10.1016/j.atmosenv.2014.11.016

Kim, S. 2011. Ozone Simulations over the Seoul Metropolitan Area for a 2007 June Episode, Part I: Evaluating Volatile Organic Compounds Emissions Speciated for the SAPRC99 Chemical Mechanism. *Journal of Korean Society for Atmospheric Environment* **27**. DOI: https://doi.org/10.5572/KOSAE.2011.27.5.580

Kim, S, Kim, SY, Lee, M, Shim, H, Wolfe, GM, Guenther, A, He, A, Hong, Y and **Han, J.** 2014. Urban-rural interactions in a South Korean forest: Uncertainties in isoprene-OH interactions limit understanding of ozone and secondary organic aerosols production. *Atmospheric Chemistry and Physics Discussions* **14**: 16691–16729. DOI: https://doi.org/10.5194/acpd-14-16691-2014

Kim, Y and **Lee, G.** 2018. Trend of Air Quality in Seoul: Policy and Science. *Aerosol and Air Quality Research* **18**. DOI: https://doi.org/10.4209/aaqr.2018.03.0081

Kleinman, L, Daum, PH, Lee, Y-N, Nunnermacker, LJ, Springston, SR, Weinstein-Lloyd, J and **Rudolph, J.** 2002. Ozone production efficiency in an urban area. *Journal of Geophysical Research: Atmospheres* **107**(D23): ACH 23-1-ACH 23–12. DOI: https://doi.org/10.1029/2002JD002529

Kleinman, L, Lee, Y-N, Springston, SR, Nunnermacker, L, Zhou, X, Brown, R, Hallock, K, Klotz, P, Leahy, D, Lee, JH and **Newman, L.** 1994. Ozone formation at a rural site in the southeastern United States. *Journal of Geophysical Research: Atmospheres* **99**(D2): 3469–3482. DOI: https://doi.org/10.1029/93JD02991

Lee, H-J, Jo, H-Y, Park, S-Y, Jo, Y-J, Jeon, W, Ahn, J-Y and **Kim, C-H.** 2019. A Case Study of the Transport/Transformation of Air Pollutants Over the Yellow Sea During the MAPS 2015 Campaign. *Journal of Geophysical Research: Atmospheres* **124**(12): 6532–6553. DOI: https://doi.org/10.1029/2018JD029751

Lee, JH, Han, JS, Yun, HK and **Cho, SY.** 2007. Evaluation of Incremental Reactivity and Ozone Production Contribution of VOCs Using the PAMS Data in Seoul Metropolitan Area. *Journal of Korean Society for Atmospheric Environment* **23**: 286–296. DOI: https://doi.org/10.5572/KOSAE.2007.23.3.286

Li, K, Jacob, DJ, Liao, H, Shen, L, Zhang, Q and **Bates, KH.** 2019. Anthropogenic drivers of 2013–2017 trends in summer surface ozone in China. *Proceedings of the National Academy of Sciences* **116**(2): 422–427. DOI: https://doi.org/10.1073/pnas.1812168116

Lin, X, Trainer, M and **Liu, SC.** 1988. On the nonlinearity of the tropospheric ozone production. *Journal of Geophysical Research: Atmospheres* **93**(D12): 15879–15888. DOI: https://doi.org/10.1029/JD093iD12p15879

Liu, SC, Trainer, M, Fehsenfeld, FC, Parrish, DD, Williams, EJ, Fahey, DW, Hübler, G and **Murphy, PC.** 1987. Ozone production in the rural troposphere and the implications for regional and global ozone distributions. *Journal of Geophysical Research: Atmospheres* **92**(D4): 4191–4207. DOI: https://doi.org/10.1029/JD092iD04p04191

Logan, JA, Prather, MJ, Wofsy, SC and **McElroy, MB.** 1981. Tropospheric chemistry: A global perspective. *Journal of Geophysical Research: Oceans* **86**(C8): 7210–7254. DOI: https://doi.org/10.1029/JC086iC08p07210

Mazzuca, GM, Ren, XR, Loughner, CP, Estes, M, Crawford, JH, Pickering, KE, Weinheimer, AJ and **Dickerson, RR.** 2016. Ozone production and its sensitivity to NO_x and VOCs: Results from the DISCOVER-AQ field experiment, Houston 2013. *Atmospheric Chemistry and Physics* **16**(22): 14463–14474. DOI: https://doi.org/10.5194/acp-16-14463-2016

Müller, M, Mikoviny, T, Feil, S, Haidacher, S, Hanel, G, Hartungen, E, Jordan, A, Märk, L, Mutschlechner, P, Schottkowsky, R, Sulzer, P, Crawford, JH and **Wisthaler, A.** 2014. A compact PTR-ToF-MS instrument for airborne measurements of volatile organic compounds at high spatiotemporal resolution. *Atmos Meas Tech* **7**(11): 3763–3772. DOI: https://doi.org/10.5194/amt-7-3763-2014

NIER and **NASA.** 2017. KORUS-AQ Rapid Science Synthesis Report. Available at https://espo.nasa.gov/sites/default/files/documents/KORUS-AQ%20RSSR.pdf (accessed November 12, 2019).

Ninneman, M, Lu, S, Lee, P, McQueen, J, Huang, J, Demerjian, K and **Schwab, J.** 2017. Observed and Model-Derived Ozone Production Efficiency over Urban and Rural New York State. *Atmosphere* **8**(7). DOI: https://doi.org/10.3390/atmos8070126

Nunnermacker, LJ, Kleinman, LI, Imre, D, Daum, PH, Lee, Y-N, Lee, J-H, Springston, SR, Newman, L and **Gillani, N.** 2000. NO_y lifetimes and O_3 production efficiencies in urban and power plant plumes: Analysis of field data. *Journal of Geophysical Research: Atmospheres* **105**(D7): 9165–9176. DOI: https://doi.org/10.1029/1999JD900753

Olszyna, KJ, Bailey Elizabeth, M, Simonaitis, R, Meagher James, F. 1994. O_3 and NO_y relationships at a rural site. *Journal of Geophysical Research: Atmospheres* **99**(D7): 14557–14563. DOI: https://doi.org/10.1029/94JD00739

Park, RJ and **Kim, S-W.** 2014. Air quality modeling in East Asia: Present issues and future directions. *Asia-Pacific Journal of Atmospheric Sciences* **50**(1): 105–120. DOI: https://doi.org/10.1007/s13143-014-0030-9

Porter, WC, Safieddine, SA and **Heald, CL.** 2017. Impact of aromatics and monoterpenes on simulated tropospheric ozone and total OH reactivity. *Atmospheric Environment* **169**: 250–257. DOI: https://doi.org/10.1016/j.atmosenv.2017.08.048

Richter, D, Weibring, P, Walega, JG, Fried, A, Spuler, SM and **Taubman, MS.** 2015. Compact highly sensitive multi-species airborne mid-IR spectrometer. *Applied Physics B* **119**(1): 119–131. DOI: https://doi.org/10.1007/s00340-015-6038-8

Rickard, AR, Salisbury, G, Monks, PS, Lewis, AC, Baugitte, S, Bandy, BJ, Clemitshaw, KC and **Penkett, SA.** 2002. Comparison of measured ozone production efficiencies in the marine boundary layer at two European coastal sites under different pollution regimes. *Journal of Atmospheric Chemistry* **43**(2): 107–134. DOI: https://doi.org/10.1023/A:1019970123228

Ridley, BA and **Grahek, FE.** 1990. A Small, Low Flow, High Sensitivity Reaction Vessel for NO Chemiluminescence Detectors. *Journal of Atmospheric and Oceanic Technology* **7**(2): 307–311. DOI: https://doi.org/10.1175/1520-0426(1990)007<0307:ASLFHS>2.0.CO;2

Ryu, Y-H, Baik, J-J, Kwak, K-H, Kim, S and **Moon, N.** 2013. Impacts of urban land-surface forcing on ozone air quality in the Seoul metropolitan area. *Atmos Chem Phys* **13**(4). DOI: https://doi.org/10.5194/acp-13-2177-2013

Sarwar, G, Simon, H, Bhave, P and **Yarwood, G.** 2012. Examining the impact of heterogeneous nitryl chloride production on air quality across the United States. *Atmos Chem Phys* **12**(14): 6455–6473. DOI: https://doi.org/10.5194/acp-12-6455-2012

Scarino, AJ, Obland, MD, Fast, JD, Burton, SP, Ferrare, RA, Hostetler, CA, Berg, LK, Lefer, B, Haman, C, Hair, JW, Rogers, RR, Butler, C, Cook, AL and **Harper, DB.** 2014. Comparison of mixed layer heights from airborne high spectral resolution lidar, ground-based measurements, and the WRF-Chem model during CalNex and CARES. *Atmos Chem Phys* **14**(11): 5547–5560. DOI: https://doi.org/10.5194/acp-14-5547-2014

Schroeder, JR, Crawford, JH, Fried, A, Walega, J, Weinheimer, A, Wisthaler, A, Müller, M, Mikoviny, T, Chen, G, Shook, M, Blake, DR and **Tonnesen, GS.** 2017. New insights into the column CH_2O/NO_2 ratio as an indicator of near-surface ozone sensitivity. *Journal of Geophysical Research: Atmospheres* **122**(16): 8885–8907. DOI: https://doi.org/10.1002/2017JD026781

Shin, HJ, Kim, JC, Lee, SJ and **Kim, YP.** 2013. Evaluation of the optimum volatile organic compounds control strategy considering the formation of ozone and secondary organic aerosol in Seoul, Korea. *Environmental Science and Pollution Research* **20**(3): 1468–1481. DOI: https://doi.org/10.1007/s11356-012-1108-5

Susaya, J, Kim, K-H, Shon, Z-H and **Brown, RJC.** 2013. Demonstration of long-term increases in tropospheric O_3 levels: Causes and potential impacts. *Chemosphere* **92**(11): 1520–1528. DOI: https://doi.org/10.1016/j.chemosphere.2013.04.017

Tong, NYO, Leung, DYC and **Liu, C-H.** 2011. A Review on Ozone Evolution and Its Relationship with Boundary Layer Characteristics in Urban Environments. *Water, Air, & Soil Pollution* **214**(1): 13–36. DOI: https://doi.org/10.1007/s11270-010-0438-5

Trainer, M, Parrish, DD, Buhr, MP, Norton, RB, Fehsenfeld, FC, Anlauf, KG, Bottenheim, JW, Tang, YZ, Wiebe, HA, Roberts, JM, Tanner, RL, Newman, L, Bowersox, VC, Meagher, JF, Olszyna, KJ, Rodgers, MO, Wang, T, Berresheim, H, Demerjian,

KL and **Roychowdhury, UK.** 1993. Correlation of ozone with NO_y in photochemically aged air. *Journal of Geophysical Research: Atmospheres* **98**(D2): 2917–2925. DOI: https://doi.org/10.1029/92JD01910

Trainer, M, Parrish, DD, Goldan, PD, Roberts, J and **Fehsenfeld, FC.** 2000. Review of observation-based analysis of the regional factors influencing ozone concentrations. *Atmospheric Environment* **34**(12): 2045–2061. DOI: https://doi.org/10.1016/S1352-2310(99)00459-8

van der Werf, GR, Randerson, JT, Giglio, L, Collatz, GJ, Mu, M, Kasibhatla, PS, Morton, DC, DeFries, RS, Jin, Y and **van Leeuwen, TT.** 2010. Global fire emissions and the contribution of deforestation, savanna, forest, agricultural, and peat fires (1997–2009). *Atmos Chem Phys* **10**(23): 11707–11735. DOI: https://doi.org/10.5194/acp-10-11707-2010

WHO. 2003. Health Aspects of Air Pollution with Particulate Matter, Ozone and Nitrogen Dioxide, Report on a WHO Working Group.

Woo, J-H, Choi, K-C, Kim, HK, Baek, BH, Jang, M, Eum, J-H, Song, CH, Ma, Y-I, Sunwoo, Y, Chang, L-S and **Yood, SH.** 2012. Development of an anthropogenic emissions processing system for Asia using SMOKE. *Atmospheric Environment* **58**: 5–13. DOI: https://doi.org/10.1016/j.atmosenv.2011.10.042

Ye, C, Zhang, N, Gao, H and **Zhou, X.** 2017. Photolysis of Particulate Nitrate as a Source of HONO and NO_x. *Environmental Science & Technology* **51**(12): 6849–6856. DOI: https://doi.org/10.1021/acs.est.7b00387

Zaveri, RA, Berkowitz, CM, Kleinman, LI, Springston, SR, Doskey, PV, Lonneman, WA and **Spicer, CW.** 2003. Ozone production efficiency and NO_x depletion in an urban plume: Interpretation of field observations and implications for evaluating O_3-NO_x-VOC sensitivity. *Journal of Geophysical Research: Atmospheres* **108**(D14). DOI: https://doi.org/10.1029/2002JD003144

How to cite this article: Oak, YJ, Park, RJ, Schroeder, JR, Crawford, JH, Blake, DR, Weinheimer, AJ, Woo, J-H, Kim, S-W, Yeo, H, Fried, A, Wisthaler, A and Brune, WH. 2019. Evaluation of simulated O_3 production efficiency during the KORUS-AQ campaign: Implications for anthropogenic NO_x emissions in Korea. *Elem Sci Anth,* 7: 56. DOI: https://doi.org/10.1525/elementa.394

Domain Editor-in-Chief: Detlev Helmig, Institute of Alpine and Arctic Research, University of Colorado Boulder, US

Associate Editor: Jochen Stutz, Atmospheric and Oceanic Sciences, University of California Los Angeles, US

Knowledge Domain: Atmospheric Science

Part of an *Elementa* Special Feature: Korea-United States Air Quality (KORUS-AQ)

Submitted: 14 April 2019 **Accepted:** 14 November 2019 **Published:** 27 December 2019

ELEMENTA Science of the Anthropocene

Elem Sci Anth is a peer-reviewed open access journal published by University of California Press.

OPEN ACCESS